One-Pot Syntheses of the First Series of Emulsion Based Hierarchical Hybrid Organic−Inorganic Open-Cell Monoliths Possessing Tunable Functionality (Organo−Si(HIPE) Series)

Simona Ungureanu,[†,||] Marc Birot,[‡] Guillaume Laurent,[§] Hervé Deleuze,[‡] Odile Babot,[‡] Beatriz Julián-López,[§] Marie-France Achard,[†] Marcel Ionel Popa,[||] Clément Sanchez,*[,§] and Rénal Backov*[,†]

Centre de Recherche Paul Pascal, UPR 8641-CNRS, Université Bordeaux 1, 115 avenue Albert Schweitzer, 33600 Pessac, France, Institut des Sciences Moléculaires, UMR 5255-CNRS, Université Bordeaux 1, 351 Cours de la Libération, 33045 Talence Cedex, France, Laboratoire de Chimie de la Matière Condensée de Paris, UMR-7574 CNRS, 4 Place Jussieu, Université Pierre et Marie Curie (UPMC), France, and Facultatea Chimie Industriala, Bd. D. Mangeron, nr. 71, Iasi, 700050, Romania

Received July 24, 2007. Revised Manuscript Received August 30, 2007

The elaboration of organo−silica-based hybrid monoliths exhibiting a hierarchical trimodal porous structure (micro-, meso-, and macroporosity) with tunable functionality have been synthesized for the first time via high internal phase emulsion (HIPE) process and lyotropic mesophases. Through one-pot synthesis, many organic functionalities that can act as network modifiers (methyl, dinitrophenylamino, benzyl, and mercaptopropyl) or co-network formers (pyrrol) have been anchored to the amorphous silica porous network. The resulting materials have been thoroughly characterized via a large set of techniques: SEM, TEM, SAXS, mercury porosimetry, nitrogen adsorption isotherms, FTIR, ^{29}Si MAS NMR, and XPS. These sol−gel-derived hierarchical open-cell functional hybrid monoliths exhibit macroscopic void spaces ranging from 5 μm up to 30 μm and their accessible micro-and mesoporosities reveal hexagonal organization for the dinitrophenylamino-, benzyl-, and pyrrol-based hybrids. The average condensation degree for these hybrid networks ranges between 86 and 90%, yielding shaped monoliths with both good integrity and sufficient mechanical properties to be usable as functional catalytic or chromatographic supports. Also, function accessibility has been demonstrated through heterogeneous nucleation of Pd metallic nanoparticles.

Introduction

Bio-inspired approaches and induced bio-inspired materials have open new chemical strategies by combining mainly sol−gel or mineralization processes with templated growth.[1] The use of lyotropic mesophases (biological or not), microemulsions, and external solicitations allow, thus, through an intelligent and tuned coding, developing innovative materials having complex hierarchical architectures.[1] Current approaches to hierarchically structured inorganic materials include coupling of multiscale templating that make use of self-assembled surfactant with larger templates as emulsion droplets,[2] air−liquid foams,[3] latex beads,[4] bacterial threads,[5] organogelators,[6] controlled phase segregation,[7] and nano- and macromolding.[8] Also, all previously mentioned morphosyntheses can be achieved while employing external stimuli as for instance electric or magnetic fields,[9] fluxes,[10] mechanical constraints,[11] imprinting,[12,1c] and so forth. During the last 10 years, beyond exclusive morphogenesis approaches, research has been mainly focused on networks based on amorphous silica that can be eventually functionalized by organic groups (R), this functionalization allowing the combination at the nanosize level of inorganic and

* Authors to whom correspondence should be addressed. E-mail: backov@crpp-bordeaux.cnrs.fr (R. Backov); clems@ccr.jussieu.fr (C. Sanchez).

† Centre de Recherche Paul Pascal, UPR 8641-CNRS, Université Bordeaux 1.

‡ Institut des Sciences Moléculaires, UMR 5255-CNRS, Université Bordeaux 1.

§ Université Pierre et Marie Curie.

|| Facultatea Chimie Industriala.

(1) (a) Mann, S.; Burkett, S. L.; Davis, S. A.; Fowler, C. E.; Mendelson, N. H.; Sims, S. D.; Walsh, D.; Whilton N. T. *Chem. Mater.* **1997**, *9*, 2300. (b) Ozin, G. A. *Chem. Commun.* **2000**, *6*, 419. (c) Soler-Illia, G. J. A. A.; Sanchez, C.; Lebeau, B.; Patarin, J. *Chem. Rev.* **2002**, *102*, 4093. (d) Sanchez, C.; Arribart, H.; Giraud-Guille, M. M. *Nat. Mater.* **2005**, *4*, 277. (e) Xu, A.-W.; Ma, Y.; Cölfen, H. *J. Mater. Chem.* **2007**, *17*, 415.

(2) Imhof, A.; Pine. D. J. *Adv. Mater.* **1998**, *10*, 697.

(3) (a) Chandrappa, G. T.; Steunou, N.; Livage, J. *Nature* **2002**, *416*, 702. (b) Maekawa, H.; Esquena, J.; Bishop, S.; Solans, C.; Chmelka, B. F. *Adv. Mater.* **2003**, *15*, 591. (c) Huerta, L.; Guillem, C.; Latorre, J.; Beltran, A.; Beltran, D.; Amoros, P. *Chem. Commun.* **2003**, 1448. (d) Carn, F.; Colin, A.; Achard, M.-F.; Deleuze, H.; Saadi, Z.; Backov, R. *Adv. Mater.* **2004**, *16*, 140. (e) Walsh, D.; Kulak, A.; Aoki, K.; Ikoma, T.; Tanaka, J.; Mann, S. *Angew. Chem., Int. Ed.* **2004**, *43*, 6691. (f) Carn, F.; Masse, P.; Saadaoui, H.; Julian, B.; Deleuze, H.; Ravaine, S.; Sanchez, C.; Talham, D. R.; Backov, R. *Langmuir* **2006**, *22*, 5469. (g) Carn, F.; Achard, M.-F.; Babot, O.; Deleuze, H.; Reculusa, S.; Backov, R. *J. Mater. Chem.* **2005**, *15*, 3887.

(4) (a) Holland, B. T.; Blanford, C. F.; Stein, A. *Science* **1998**, *281*, 538. (b) Antonietti, M.; Berton, B.; Göltner, C.; Henz, H.-P. *Adv. Mater.* **1998**, *10*, 154.

(5) Davis, S. A.; Burkett, S. L.; Mendelson, N. H.; Mann, S. *Nature* **1997**, *385*, 420.

(6) Llusar, M.; Roux, C.; Pozzo, J.-L.; Sanchez, C. *J. Mater. Chem.* **2003**, *3*, 442.

(7) Nakanishi, N. *J. Porous Mater.* **1997**, *4*, 67.

(8) (a) Yang, P.; Deng, T.; Zhao, D.; Feng, P.; Pine, D.; Scmelka, B. F.; Whitesides, G. M.; Stucky, G. D. *Science* **1998**, *282*, 2244. (b) Wang, D.; Caruso, R. A.; Caruso, F. *Chem. Mater.* **2001**, *13*, 364.

10.1021/cm701984t CCC: $37.00
Published on Web 10/12/2007

Scheme 1. Different Organo−Silanes Mixed with TEOS as Precursors

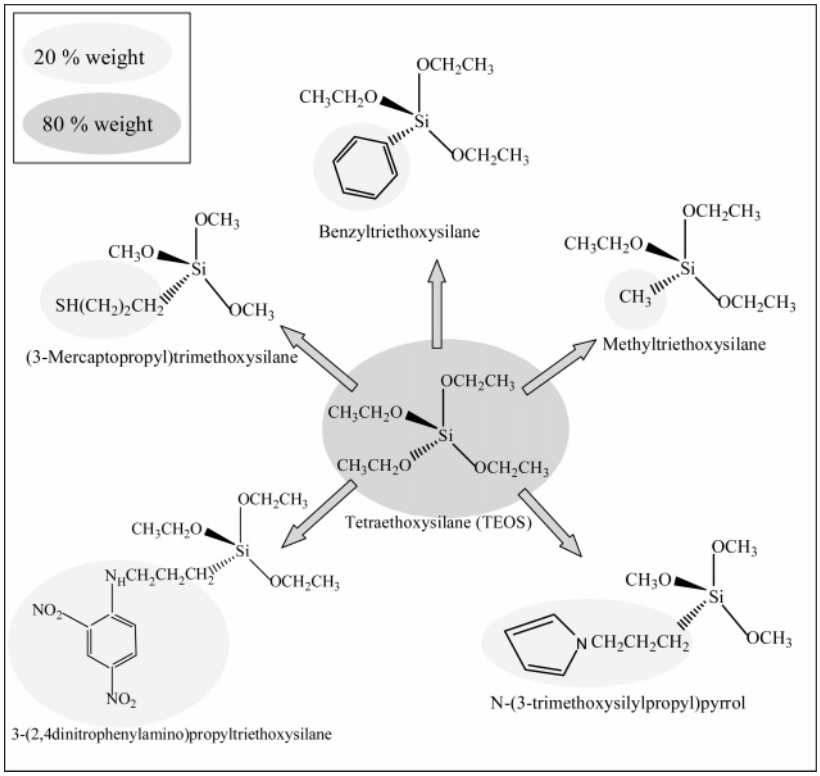

organic or even bioactive components.[13,14] These hybrids are considered as innovative advanced materials, and promising applications are expected in many fields: optics, electronics, ionics, mechanics, membranes, protective coatings, catalysis, sensors, and biology.[15,16] However, nowadays, it still appears important to achieve better control of the organization mechanisms to prepare efficient complex structures while maintaining organic moieties integrity and accessibility. Recently, from the interface between bio-inspired approaches, hybrid organic−inorganic chemistry, when extended to soft chemistry in general (including organic polymer and supramolecular chemistry) and complex fluids, has emerged the "Integrative Chemistry"[17] concept where chemistry and process are strongly coupled. More importantly, the assembly of a large variety of molecular precursors or nanobuilding blocks, through application of the "Integrative Chemistry" concept, into engineered hierarchical structures (bio-inspired or not) should be strongly pre-dictated in view of final function or polyfunctionalities to be reached and not vice versa. Particularly, ordered macro- and mesoporous materials are of interest for multiple applications in heterogeneous catalysis, separation techniques, absorbers, sensors, optics, etc. One way of generating such architectures is to use either direct concentrated nonaqueous[18] or aqueous emulsions.[19] More recently, porous silica has been prepared through water/oil emulsions stabilized by silica nanoparticles in the absence of surfactants.[20] Indeed, different silica beds have been obtained by using emulsion−polymer double templates,[21] and their interest specially lies on their high internal surface. With this aim, our research group has developed a new process to obtain macrocellular silica monoliths with high control of the final macroscopic cells (size and morphology) by playing with the oil volume fraction of the starting concentrated direct emulsions. This new series of silica porous networks were labeled Si(HIPE)[22] with regard to the first generation of porous organic polymer obtained through the use of concentrated reverse emulsions, porous polymers called Poly-HIPE, "High Internal Phase Emulsion" phases.[23]

(9) (a) Busch, S.; Dolhaine, H.; DuChesne, A.; Heinz, S.; Hochrein, O.; Laeri, F.; Podebrad, O.; Vietze, U.; Weiland, T.; Kniep, R. *Eur. J. Inorg. Chem*. **1999**, *10*, 1643. (b) Kniep, R.; Busch, S. *Angew. Chem., Int. Ed. Engl*. **1996**, *35*, 2624. (c) Terao, T.; Nakayama, T. *Phys. Rev. E*. **1999**, *60*, 7157. (d) Grzybowski, B. A.; Stone, H. A.; Whitesides, G. M. *Nature* **2000**, *405*, 1033. (e) Assi, F.; Jenks, R.; Yang, J.; Love, C.; Prentiss, M. *J. Appl. Phys*. **2002**, *92*, 5584. (f) Carn, F.; Colin, A.; Schmidt, V.; Calderon, F.-L.; Backov, R. *Colloids Surf., A* **2005**, *263*, 341.
(10) (a) Biette, L.; Carn, F.; Maugey, M.; Achard, M.-F.; Maquet, J.; Steunou, N.; Livage, J.; Serier, S.; Backov, R. *Adv. Mater*. **2005**, *17*, 2970. (b) Serier, H.; Achard, M.-F.; Steunou, N.; Maquet, J.; Livage, J.; Babot, O.; Backov, R. *Adv. Funct. Mater*. **2006**, *16*, 1745. (c) Leroy, C. M.; Achard, M.-F.; Babot, O.; Steunou, N.; Masse, P.; Livage, J.; Binet, L.; Brun, N.; Backov, R. *Chem. Mater*. **2007**, *19*, 3988.
(11) Chronakis, I. S. *J. Mater. Process. Technol*. **2005**, *167*, 283.
(12) Li, Z.; Jaroniec, M. *J. Phys. Chem. B* **2004**, *108*, 824.
(13) Sanchez, C.; Soler-Illia, G. J. A. A.; Ribot, F.; Grosso, D. *C. R. Acad. Sci. Chimie* **2003**, *8*, 109.
(14) Sanchez, C.; Soler-Illia, G. J. A. A.; Ribot, F.; Lalot, T.; Mayer, C. R.; Cabuil, V. *Chem. Mater*. **2001**, *13*, 3061.
(15) Sanchez, C.; Julian, B.; Belleville, P.; Popall, M. *J. Mater. Chem*. **2005**, *15*, 3559.
(16) (a) *Functional Hybrid Materials*; Gómez-Romero, P., Sanchez, C., Eds.; Wiley-VCH: Weinheim, 2003. (b) Sanchez, C.; Lebeau, B.; Chaput, F.; Boilot, J.-P. *Adv. Mater*. **2003**, *15*, 1969.
(17) Backov, R. *Soft Mater*. **2006**, *2*, 452.
(18) Imhof, A.; Pine, D. J. *Nature* **1997**, *389*, 948.
(19) Yi, G.-R.; Yang, S. M. *Chem. Mater*. **1999**, *11*, 2322.
(20) Binks, B. P. *Adv. Mater*. **2002**, *14*, 1824.
(21) Zhang, H.; Hardy, G. C.; Rosseinsky, M. J.; Copper, A. I. *Adv. Mater*. **2003**, *15*, 78.
(22) Carn, F.; Colin, A.; Achard, M.-F.; Deleuze, H.; Birot, M.; Backov, R. *J. Mater. Chem*. **2004**, *14*, 1370.
(23) Barby, D.; Haq, Z. Eur. Pat. 0060138, 1982.

Table 1. Organically Derived Silane Used as Precursors and Their Associated Final Hybrid Compounds

organically derived silane incorporated	final porous silica-based monoliths
benzyltriethoxysilane	benzyl−Si(HIPE)
3-(mercaptopropyl)trimethoxysilane	mercapto−Si(HIPE)
3-(2,4-dinitrophenylamino)propyltriethoxysilane	dinitro−Si(HIPE)
N-(3-trimethoxysilylpropyl)pyrrol	pyrrol−Si(HIPE)
methyltriethoxysilane	methyl−Si(HIPE)

Herein, we present for the first time a one-step method to prepare hybrid organic−inorganic porous silica-based monoliths bearing a trimodal porous structure where hierarchical architecture is triggered by the combination of a direct water/oil concentrated emulsion at the macroscopic scale and a supramolecular surfactant organization at the mesoscopic scale. The synthesis procedure is simple, does not require special handling, and allows adjustment of precise functionality at the molecular level. Moreover, the described process can easily be scaled up to larger hybrid monoliths, therefore opening the route to industrial applications.

Experimental Section

Materials. Tetraethylorthosilane (TEOS) and tetradecyltrimethylammonium bromide (TTAB) have been purchased from Fluka. (3-Mercaptopropyl)trimethoxysilane, 95%, was purchased from Lancaster. Sodium borohydride ($NaBH_4$) and dodecane were purchased from Aldrich. The methyltriethoxysilane, 98%, was purchased from Organics. The 3-(2,4-dinitrophenylamino)-propyltriethoxysilane, 95%, and the *N*-(3-trimethoxysilylpropyl)pyrrol were purchased from Gelest, Inc. Palladium tetrachloropalladate and tetrahydrofuran, 99% (THF), were purchased from Acros. All materials were used as received without further purification.

Syntheses. *R−Si(HIPE) Synthesis*. The preparation of the hybrid monoliths was performed following the same protocol but with modification of the nature of the organosilane (depicted in Scheme 1 and Table 1) in each case. In a typical synthesis, 4.03 g of TEOS and 1.01 g of the corresponding organosilane are introduced in 16.05 g of a TTAB aqueous solution at 35 wt % previously acidified (5.9 g of HCl), and hydrolysis is allowed to perform until a monophasic hydrophilic medium is obtained. When the organosilane amount is increased above 20 wt % (TEOS 80 wt %), the texture at the macroscopic length scale is lost and the monolith scaffolds collapse; i.e., we obtained powders. The oily phase constituted of 40.02 g of dodecane is then emulsified drop by drop into the hydrophilic continuous phase using a mortar. The emulsion is then allowed to condense for 1 week at room temperature. The as-synthesized monolith is washed three times with tetrahydrofuran (THF) and a last time with a THF/ethanol mixture (at 50 vol %) to extract the oily (dodecane) phase from the monolith. The drying overnight of the material is followed by further thermal treatment at 180 °C for 6 h (heating rate of 2 °C/min) to favor solvent evaporation and the consolidation of the networks.

Palladium Nanoparticles Generation. Dissolved oxygen was removed from water by bubbling argon gas for 30 min. Then K_2PdCl_4 (33.3 mg) was dissolved in 10 mL of a water/THF mixture (1:1, w/w) to get a final concentration of 10^{-2} M. To help fill up the porous matrices, a vacuum can be applied to the end of the native effervescence. Then, a fresh solution of $NaBH_4$ is prepared (130 mg of $NaBH_4$ into 10 mL of the water/THF mixture). The imbibed porous monoliths are then immerged within the as-prepared reducing solution, resulting in the monolith color change from a white/yellow to a deep brown/dark color.

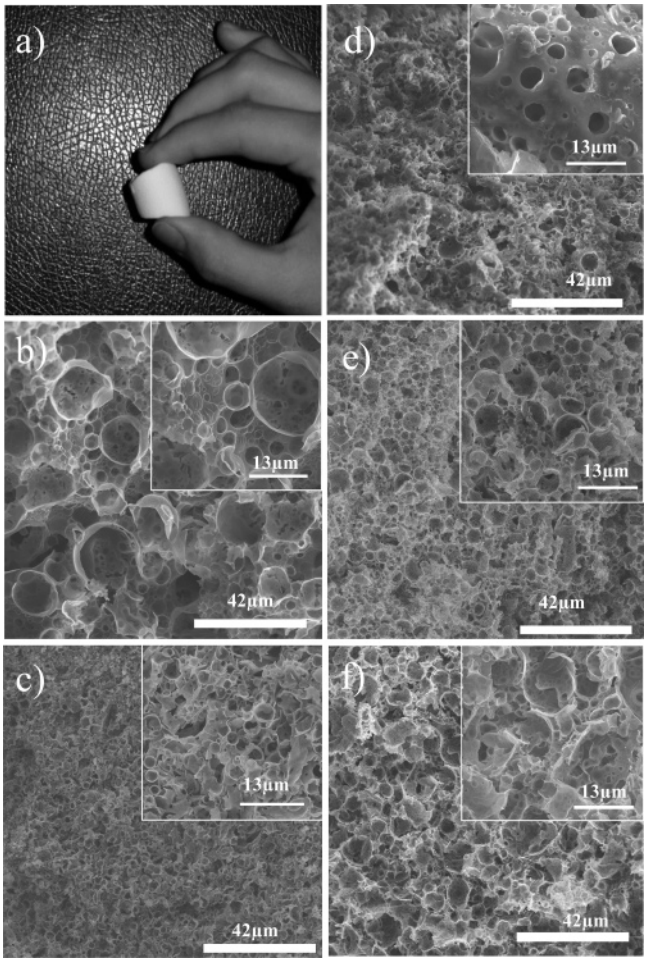

Figure 1. (a) Photograph of the as-synthesized pyrrol−Si(HIPE) compounds obtained as a monolith. SEM micrographs: (b) pyrrol−Si(HIPE), (c) methyl−Si(HIPE), (d) dinitro−Si(HIPE), (e) benzyl−Si(HIPE), and (f) mercapto−Si(HIPE).

Characterization. Transmission electron microscopy (TEM) experiments were performed with a Jeol 2000 FX microscope (accelerating voltage of 200 kV). The samples were prepared as follows: silica scaffolds in a powder state were deposited on a copper grid coated with a Formvar/carbon membrane. Scanning electron microscopy (SEM) observations were performed with a Jeol JSM-840A scanning electron microscope operating at 10 kV. The specimens were gold-coated or carbon-coated prior to examination. Surface areas and pore characteristics at the mesoscale were obtained with a Micromeritics ASAP 2010. Intrusion/extrusion mercury measurements were performed using a Micromeritics Autopore IV apparatus, this to reach the scaffolds macrocellular cells characteristics. X-ray photoelectron spectroscopy (XPS) experiments were performed using Escalab VG 220i XL apparatus. Small-angle X-ray scattering (SAXS) experiments were carried out on a 18 kW rotating anode X-ray source (Rigaku-200) with use of a Ge(111) crystal as a monochromator. The scattered radiation was collected on a two-dimensional detector (Imaging Plate system from Mar Research, Hamburg). The sample−detector distance was 500 mm. Thermogravimetric analyses (TGA) were carried out under an oxygen flux (5 $cm^3 \cdot min^{-1}$) using a heating rate of 5 $°C \cdot min^{-1}$. The apparatus is a Stearam TAG-1750 thermogravimetric analyzer. The Fourier transform infrared spectroscopy (FTIR) spectra have been obtained with a Nicolet 750 FTIR spectrometer. The ^{29}Si MAS NMR (magic angle spinning nuclear magnetic resonance) spectra were recorded on a Bruker Advance 300 spectrometer (7.04 T) operating at 59.63 MHz, with a 90° pulse of 5 μs and a recycle delay of 150 s. Samples were spun at 5 kHz using 7 mm ZrO_2

rotors. A ^{29}Si CP MAS NMR (cross polarization) spectrum was performed with $\omega_{1I}/2\pi$ and $\omega_{1S}/2\pi$ equal to 50 kHz, a contact time of 2 ms, and a recycling delay of 3 s. ^{1}H TPPM15 decoupling (two-pulse phase modulation)[24] at $\omega_{1I}/2\pi$ equal to 50 kHz was always applied during acquisition but not during recycling. Si sites are labeled with the conventional T^n and Q^n notation. T refers to functional $(R)SiO_3-$ units and Q to SiO_4- units, and n is the number of bridging oxygen atoms surrounding the silicium. The ^{13}C CP MAS NMR spectra were recorded on a Bruker Advance 400 spectrometer (9.40 T) operating at 100.61 MHz, with a 90° pulse of 2.9 μs, $\omega_{1I}/2\pi$ and $\omega_{1S}/2\pi$ equal to 50 kHz, a contact time of 1 ms, and a recycling delay of 3 s. Samples were spun at 5 or 14 kHz using 4 mm ZrO_2 rotors. ^{1}H TPPM15 at $\omega_{1I}/2\pi$ equal to 86 kHz was always applied during acquisition but not during recycling. Chemical shifts were determined relative to TMS (tetramethylsilane). The spectra were simulated with the DMFIT program.[29]

Results and Discussion

Functionalization that makes use of a co-condensation ("one-pot") process where the entity $(R-Si(OEt)_3)$ is incorporated in the reaction medium and participates in the entire synthesis has been investigated for providing optimized properties and new functionalities to multiscale organized porous silica networks. To incorporate functionalities into final porous materials, we added different organically modified silanes besides the tetraethoxyorthosilane (TEOS). A 20 and 80 wt % ratio of these molecular species were respectively introduced into the starting emulsion (Scheme 1); see Experimental Section for details.

The final porous monoliths obtained from the mixture of the aforementioned silanes are labeled as indicated in Table 1.

Characterization at the Macroscopic Length Scale. As the macroscopic length scale pattern takes advantage of concentrated direct emulsion, i.e., dispersion of oil in water, the continuous phase will be the hydrophilic media containing the hydrolyzed precursors. When the monoliths are dried, further thermal treatment at 180 °C is applied to both "remove" remnant organic solvents and consolidate the inorganic walls. In this issue it has been proven that a 150 °C thermal cure can optimize the condensation up to 5%.[25] Also, it is important to obtain monolith-type materials (Figure 1a) since it usually indicates interconnected macroporosity (Figures 1b−1f).

The first observation emerging from Figures 1b−1f is that the macroscopic void spaces are not monodisperse in size but rather polydisperse, ranging from 5 μm up to 30 μm. The macroscopic textures of the monoliths resemble a "hollow spheres" aggregation, except for the materials dinitro−Si(HIPE) (Figure 1d). As previously used to generate the Si-HIPE0.035,[22] the high acidic concentration yields the silica far from its isoelectric point and therefore the native object will depict a strong Euclidian character.[26] For the (2,4-

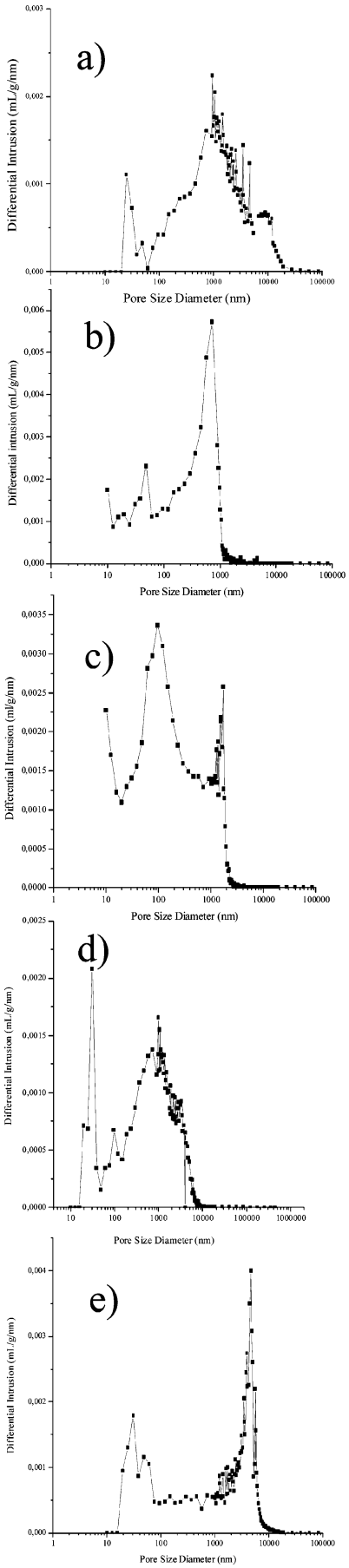

Figure 2. Macroscopic pore sizes distribution obtained through mercury intrusion porosimetry: (a) pyrrol−Si(HIPE), (b) methyl−Si(HIPE), (c) dinitro−Si(HIPE), (d) benzyl−Si(HIPE), and (e) mercapto−Si(HIPE).

(24) Bennett, A. E.; Rienstra, C. M.; Auger, M.; Lakshmi, K. V.; Griffin, R. G. *J. Chem. Phys* **1995**, *103*, 6951.
(25) Lebeau, G.; Maquet, J.; Sanchez, C.; Beaume, F.; Lauprêtre, F. *J. Mater. Chem*. **1997**, *7*, 989.
(26) Brinker, C. J.; Scherer G. W. In *Sol-Gel Science: the Physics and Chemistry of Sol-Gel Processing*; Academic Press: San Diego, 1990.

Table 2. Mercury Intrusion Porosimetry Data

materials	pyrrol−Si(HIPE)	methyl−Si(HIPE)	dinitro−Si(HIPE)	benzyl−Si(HIPE)	mercapto−Si(HIPE)
intrusion volume ($cm^3 \cdot g^{-1}$)	13.7	3.6	3.38	5.12	9.92
porosity (%)	96.2	80	92	89.4	93
bulk density ($g \cdot cm^{-3}$)	0.07	0.22	0.27	0.17	0.09
skeletal density ($g \cdot cm^{-3}$)	1.86	1.13	1.64	1.65	1.36

dinitrophenylamino)propyltriethoxysilane entities used with the same HCl concentration, the pH after hydrolysis evolves from 0.04 to 0.4, reaching thus values closer to the silica isoelectric point. As demonstrated elsewhere,[22] in such condition, the pH value closer to the silica isoelectric point will induce a higher fractal character where the continuous aqueous media will be fully mineralized (Figure 1d). Also, as previously mentioned it is obvious that mineralization starts at the oil/water interface and then extends to the aqueous hydrophilic phase, the interface acting as a defect where the nucleation enthalpy will be lowered. Beyond SEM observations it is important to provide more quantitative information related to the macroporosity, as for instance bulk and skeleton densities. With this purpose, we performed mercury porosimetry on these supports. The first piece of information that is of importance for further applications is the fact that these as-synthesized materials possess mechanical strength high enough to support mercury impregnation. Also, we have to bear in mind that mercury porosimetry provides information only on the features that control the mercury impregnation, i.e., the windows that connect two adjacent macropores, rather than the macropore diameters themselves. As previously observed for the inorganic Si-HIPE series, we obtain two sets of windows. First, we have the windows that intrinsically connect two adjacent macropores that we have previously called "internal junctions".[22] Also, considering the aggregated "hollow spheres" textural aspect of the macropores, we are obliged to consider windows emerging from aggregation between several hollow spheres; this is what we have previously called "external junctions". At that point, it is expected to get two main contributions when considering the cell-junction diameters distribution data when the "hollow sphere" textural aspect is obvious; this effect is even clearly seen in Figure 2.

On the other hand, the macropores distribution becomes narrower when considering the material dinitro−Si(HIPE), as the continuous aqueous phase is more completely mineralized and the aggregated "hollow sphere" character is practically lost (Figure 1d), for the reason explained above, i.e., walls enhanced fractal character. Specific morphological characteristics (percentage of porosity, bulk, and skeleton densities) of these hybrid compounds can be found in Table 2.

Characterization at the Mesoscopic Length Scale. At the mesoscopic length scale these hybrid organic−inorganic porous monoliths possess a secondary porosity. This mesoporosity can be first observed using TEM investigations and qualified using SAXS experiments (Figure 3). First, we notice that mesoporosity is present for all the as-synthesized compounds as observed by TEM experiments. This mesoporosity is characteristic of randomly dispersed pores for the materials methyl−Si(HIPE) and mercapto−Si(HIPE) while other hybrid compounds reveal a hexagonal organization (Figures 3a−3e). This visual information is also relayed when performing SAXS experiments that confirm either the poor organization (Figures 3g and 3j) without diffusion pattern from 0.5 to 0.2 q($Å^{-1}$) or characteristic diffusion peaks with their harmonics that correspond to a hexagonal mesoscopic

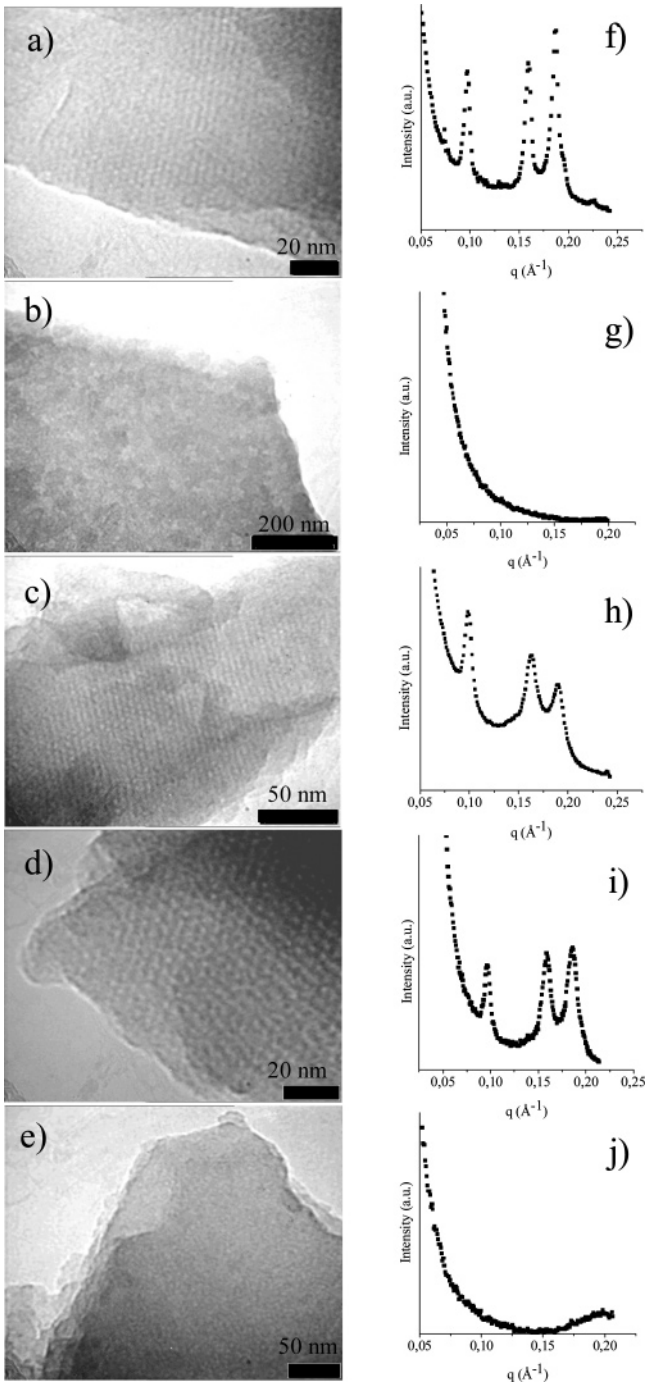

Figure 3. (a−e) TEM pictures of the as-synthesized materials walls: (a) pyrrol−Si(HIPE), (b) methyl−Si(HIPE), (c) dinitro−Si(HIPE), (d) benzyl−Si(HIPE), and (e) mercapto−Si(HIPE). (f−j) SAXS diffusion profiles of the organo−Si(HIPE) series: (f) pyrrol−Si(HIPE), (g) methyl−Si(HIPE), (h) dinitro−Si(HIPE), (i) benzyl−Si(HIPE), and (j) mercapto−Si(HIPE).

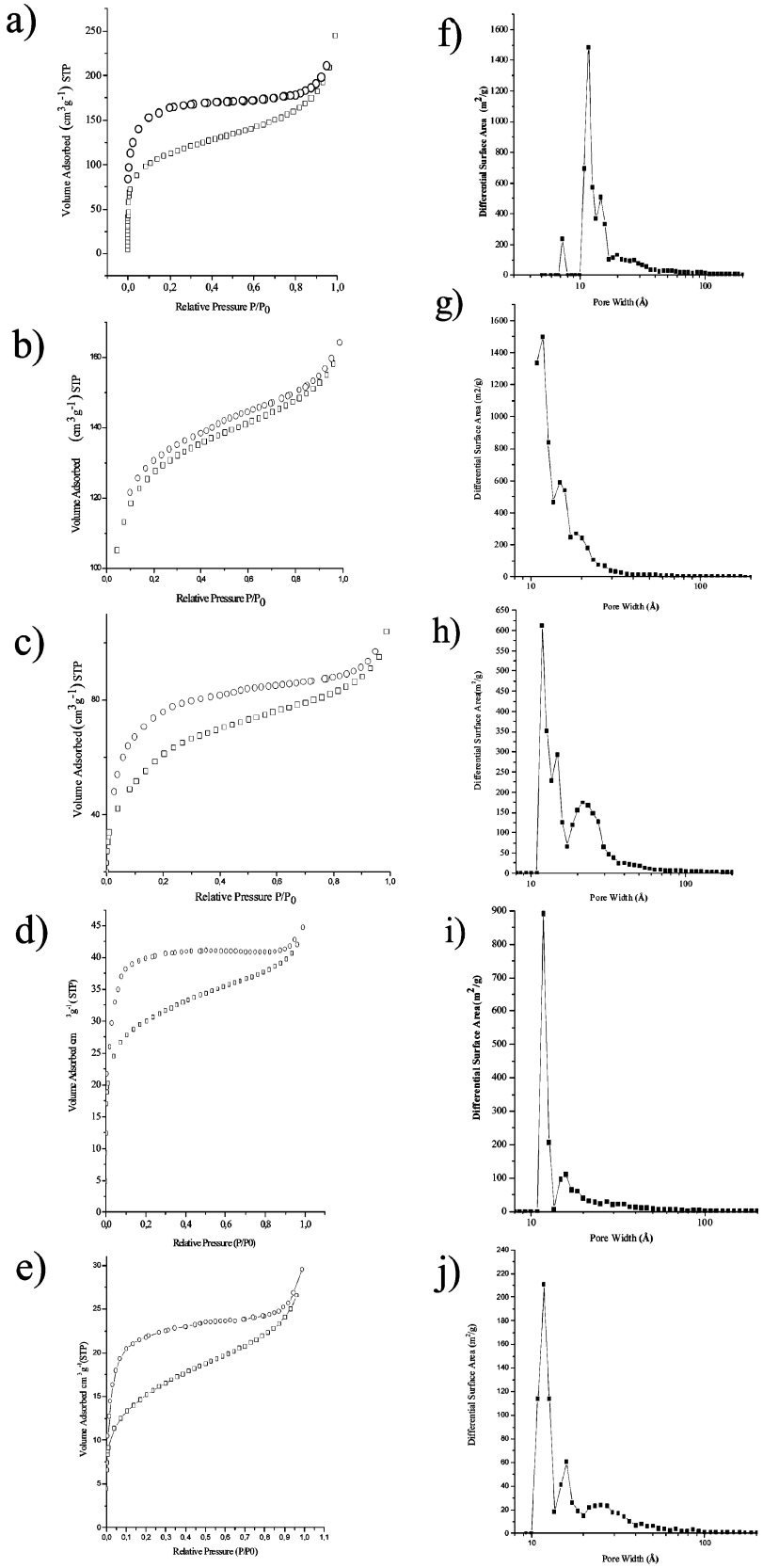

Figure 4. Nitrogen adsorption−desorption curves: (a) pyrrol−Si(HIPE), (b) methyl−Si(HIPE), (c) dinitro−Si(HIPE), (d) benzyl−Si(HIPE), (e) mercapto−Si(HIPE). □, adsorption curve; ○, desorption curve. Mesoscopic and microscopic pore sizes distribution obtained through the differential functional theory (DFT): (a) pyrrol−Si(HIPE), (b) methyl−Si(HIPE), (c) dinitro−Si(HIPE), (d) benzyl−Si(HIPE), and (e) mercapto−Si(HIPE).

void spaces organization (Figures 3f, 3h, and 3i). This difference of organization is certainly not imposed by the Lewis base character as the mercapto derivative does not offer high organization contrary to what is observed for organic moieties bearing amino derivatives, i.e., pyrrol−Si(HIPE) and dinitro−Si(HIPE). Also, we have to notice that the benzyl derivative is associated with a mesoscopic structural effect while the methyl silane one is not, as seen

Table 3. Hybrid Monoliths Surface Area Calculated from Both the BET and BJH Methods[a]

materials	pyrrol−Si(HIPE)	methyl−Si(HIPE)	dinitro−Si(HIPE)	benzyl−Si(HIPE)	mercapto−Si(HIPE)
BET ($m^2 \cdot g^{-1}$)	392	450	217	107	53
BJH ($m^2 \cdot g^{-1}$)	83	98	87	14	15
total pore volume (cm^3/g)	0.38	0.25	0.16	0.07	0.05

[a] The BJH method is applied only to pore sizes higher than 35 Å and for the desorption curve.

in Figures 3i and 3g, respectively. Considering the whole organo−silane derivatives, this is the one possessing the ability of being protonated under acidic conditions which promotes higher organization, i.e., organic moieties bearing amino or phenyl groups. In this way pyrrol, dinitro, and phenyl silane derivatives may act as co-surfactants that help stabilize the interface between the native mixed micelles and the on-growing organo−silica network. Furthermore, considering the benzyl organosilane derivatives, Babonneau et al. have demonstrated the capability of aromatic organo silanes to induce enhanced mesoscopic organization.[27] Also, it is important to have a close look at the hexagonal unit cell extracted from the SAXS experiments. Typically, a first peak is observed for 6.5 nm (0.096 $Å^{-1}$) associated with two other contributions at 3.9 nm (0.159 $Å^{-1}$) and 3.4 nm (0.185 $Å^{-1}$). The presence of these last two peaks is suggestive of a hexagonal organization of the channels, and it has been reported that the SAXS spectrum of powdery hexagonal mesoporous materials exhibits a typical three peak pattern, associated with a first feature at low angle (100 reflection line) and two other peaks at higher angles (110 and 200 reflections lines).[28] These three reflection lines can be attributed to a hexagonal unit cell ($a_0 = 2d_{100}/3^{1/2}$), which corresponds to the sum of the pore diameter and the pore wall thickness. According to Bragg's law, the unit cell dimension (a_0) for the compounds is found to be the same and equals 7.5 nm. A previous study, considering the same surfactant in use, tetradecyltrimethylammonium bromide (TTAB), under the same pH conditions for the generation of the purely inorganic Si-HIPE materials,[22] showed a mesoscale wall-to-wall vermicular distance of 4.8 nm, which offers a discrepancy of 2.7 nm with the present results. In fact, for the organized compounds pyrrol−Si(HIPE), dinitro−Si(HIPE), and benzyl−Si(HIPE), as expressed above, we cannot consider the TTAB micelles only to organize the compounds mesoporosity, but rather mixed (TTAB/organosilane derivative) micelles, certainly with some swollen effect coming from the encapsulation of dodecane, i.e., the oily phase that has been emulsified to generate the macroporosity. The capabilities to generate these microemulsions will increase with the stability of the micellar systems in use.

To better describe the mesoscale void space organization and quantify the associated specific surface areas, nitrogen adsorption−desorption measurements were performed at 77 K on materials thermally treated at 180 °C. All the nitrogen adsorption−desorption curves are depicted within Figures 4a−4e.

In a general manner, N_2 adsorption curves rise rapidly in the low relative pressure range (0 to 0.3) followed by some more nitrogen adsorption at higher relative pressure values, indicating thus the presence of a textural microporosity. Above a relative pressure of 0.3 and up to 1.0 a distinct hysteresis loop can be observed between the adsorption and desorption curves that confirmed the presence of mesopore within the different samples. Table 3 summarizes the specific surface areas of the different thermally treated hybrid monoliths when using both the BET and BJH methods. Considering Table 3, we can consider that the hybrid compounds are essentially microporous (pore sizes between 12 and 20 Å) associated to some degree with mesoporosity (pore sizes higher than 35 Å).

Also, pore sizes distributions have been expressed using the density functional theory (DFT) method (Figures 4f−4j). In good relation with what observed and extracted from the nitrogen physisorption experiments, all the pore sizes distribution are depicting a bimodal pore sizes distribution with basically two main contributions around 1.1 and 2.2 nm, with some residual mesoporosity. At this stage, if we compared the nitrogen physisorption results, which strongly suggest microporosity, with the SAXS experiments that reveal, for the organized compound, a structural unit cell a_0 equal to 7.5 nm, there is, at first glance, a certain discrepancy as we might expect from the SAXS experiments a strong mesoposity emerging from the BJH calculations. In fact, as discussed later within the FTIR spectroscopy section, both organic moieties (R) of the silane groups and some surfactant remain intact through the THF washing process and the applied thermal treatment (6 h at 180 °C). As a direct consequence, the porosity and associated pore sizes distribution observed through nitrogen adsorption−desorption is only the void space diameter (1.5−2 nm) emerging through the dodecane droplets departure, dodecane involved within the native microemulsions. Finally, if we add 2 times the TTAB long axis (4 nm, being the mixed micelle higher diameter), the swollen effect induced by some embedded dodecane (1.5−2 nm) and the wall thickness (1.5−2 nm), we recover a unit cell a_0 of 7−8 nm that corresponds to the SAXS results (a_0 equal to 7.5 nm).

Characterization at the Microscopic Length Scale. The synthesis of these hierarchical open-cell functional hybrid monoliths via sol−gel involves hydrolysis and condensation of different precursors, bearing different hydrolysis−condensation kinetics when compared with TEOS. Since TEOS and organosilanes present large differences in chemical reactivity, it is important to know the co-condensation degree of the silicate species in the final monoliths. Solid-state ^{29}Si NMR appears as a straightforward tool to probe the local chemical environment around the Si atoms and, therefore, it allows identification and quantification of the

(27) Babonneau, F.; Leite, L.; Fontlupt, S. *J. Mater. Chem.* **1999**, *9*, 175.
(28) Chen, C. Y.; Xiao, S. O.; Davis, M. E. *Microporous Mater.* **1995**, *5*, 20.

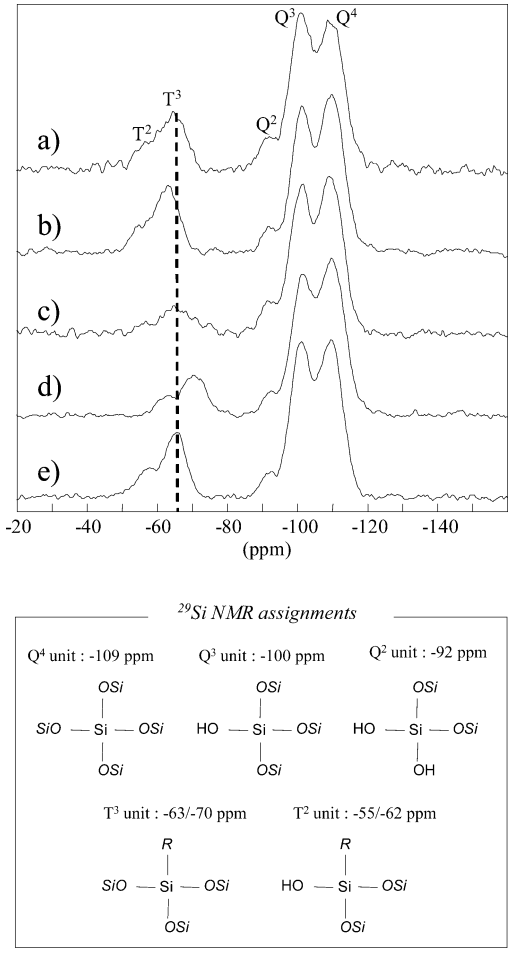

Figure 5. ^{29}Si MAS NMR spectra of the as-synthesized hybrid monoliths and the assignments of the signals to silane-derived species: (a) pyrrol−Si(HIPE), (b) methyl−Si(HIPE), (c) dinitro−Si(HIPE), (d) benzyl−Si(HIPE), and (e) mercapto−Si(HIPE).

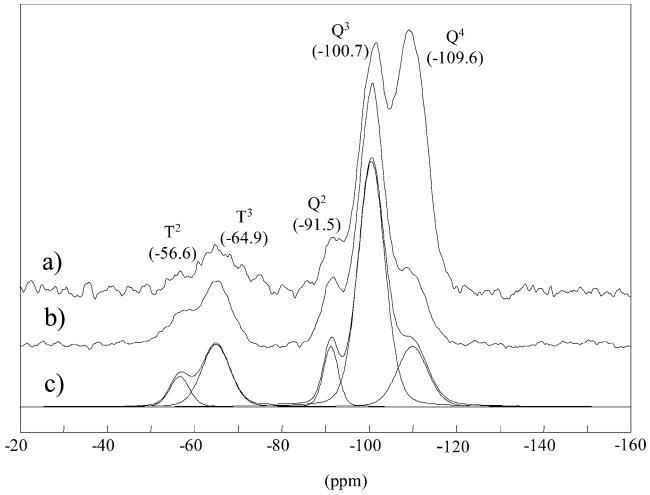

Figure 6. (a) Experimental ^{29}Si MAS: (b) CP MAS NMR and (c) simulated ^{29}Si CP MAS NMR spectrum of dinitro−Si(HIPE) sample.

different siloxane species. Figure 5 illustrates the ^{29}Si MAS NMR spectra recorded for the samples. Assignments of the ^{29}Si NMR signals to the silicate species according to the conventional notation have also been included.

All spectra show two groups of signals at chemical shifts (δ) of around −60/−70 ppm and −100/−110 ppm, characteristic of the T and Q units,[29,30] respectively. The presence of not fully O bridging silane species, i.e., Q^2 (−92 ppm), Q^3 (−100 ppm), and T^2 (−55/−62 ppm) units, besides those of Q^4 (−109 ppm) and T^3 (−62/−70 ppm) units, indicates that the organically modified silica is not completely condensed. On the other hand, it must be noticed that while Q^n signals appear at the same chemical shift in all the spectra, the position of T^n units significantly varies depending on the hybrid system. The shift in the signal position is related to the modification of the Si surroundings because of the different electronic inductive effects of the organic moieties bonded to the silicon atom. In particular, electron-withdrawing groups such as benzyl induce a shift toward lower chemical shifts and vice versa (see dotted line in Figure 5). Quantitative analysis of the ^{29}Si MAS NMR spectra was performed by fitting the spectra with the DMFIT program.[31] Simulation consists of decomposing each spectrum in standard Gaussian/Lorentzian curves corresponding to the different Q and T signals, as illustrated in Figure 6.

The parameters obtained from these simulations, namely, the chemical shift and the percentage of each silicate unit, will provide indispensable information for the structural characterization of the hybrid monoliths. In the case of the dinitro−Si(HIPE) spectrum, in which T units are not well-resolved, an additional ^{29}Si CP-MAS NMR experiment was performed to determine the precise position of the signals and the MAS NMR spectrum was fitted keeping the same position and line with values (Figure 6). Table 4 reports the chemical shift (ppm), surface area (%), and line widths (ppm)

Table 4. Characteristic Parameters of R−Si(HIPE) Monoliths Obtained from Simulation of ^{29}Si NMR Spectra: Chemical Shift (δ), Relative Percentage (P) and Line Width (LW)

sample	δ/ppm (±0.5)	P/% (±1)	LW/ppm (±0.2)
pyrrol−Si(HIPE)	−56.6	4.5	5.3
	−64.6	14.7	7.6
	−91.4	3.9	4.0
	−100.8	36.4	7.3
	−109.9	40.5	8.2
methyl−Si(HIPE)	−54.9	4.0	5.3
	−62.8	17.4	7.6
	−91.6	2.5	4.0
	−101.1	32.7	7.3
	−110.0	43.4	8.2
dinitro−Si(HIPE)	−56.6	1.6	5.3
	−64.9	8.0	7.6
	−91.5	4.3	4.0
	−100.7	37.8	7.3
	−109.6	48.3	8.2
benzyl−Si(HIPE)	−62.1	3.1	5.3
	−70.5	11.5	7.6
	−92.0	2.6	4.0
	−101.3	35.5	7.3
	−110.1	47.3	8.2
mercapto−Si(HIPE)	−56.4	4.4	5.3
	−65.0	16.3	7.6
	−91.4	2.4	4.0
	−100.8	35.1	7.3
	−109.6	41.8	8.2

(29) (a) Harris, R. K.; Robbins, M. L. *Polymer* **1978**, *19*, 1123. (b) Babonneau, F. *New J. Chem.* **1994**, *18*, 1065. (c) Chevalier, Y.; Grillet, A.-C.; Rahmi, M.-I.; Lière, C.; Masure, M.; Hémery, P.; Babonneau, F. *Mater. Sci. Eng. C* **2002**, *21*, 143.
(30) Glaser, R. H.; Wilkes, G. L.; Bronnimann, C. E. *J. Non-Cryst. Solids* **1989**, *113*, 73.
(31) Massiot, D.; Fayon, F.; Capron, M.; King, I.; Le Calvé, S.; Alonso, B.; Durand, J.; Bujoli, B.; Ghan, Z.; Hoatson, G. *Magn. Reson. Chem.* **2002**, *20*, 70.

Table 5. Molar Percentages of Initial Precursors (TEOS and Organosilanes), Q ($Q^2 + Q^3 + Q^4$) and T ($T^2 + T^3$) Units from Simulations, and Condensation Degree (in %) of the As-Synthesized Monoliths

sample	% TEOS	% R−silane	% Q units	% T units	C.D.^{Q} (%)	C.D.^{T} (%)	C.D. (%)
pyrrol−Si(HIPE)	81.4	18.6	80.8	19.2	86.3	92.2	87.2
methyl−Si(HIPE)	77.0	23.0	78.6	21.4	88.0	93.8	89.0
dinitro−Si(HIPE)	88.1	11.9	90.4	9.6	87.2	94.4	87.7
benzyl−Si(HIPE)	82.5	17.5	85.4	14.6	88.1	92.9	88.6
mercapto−Si(HIPE)	78.8	21.2	79.3	20.7	87.4	92.9	88.3

Table 6. Stoichiometry of the Obtained Open-Cell Monoliths Organo−SiHIPE Series[a]

sample	organic weight loss[b] (%)	water weight loss[b] (%)	stoichiometry
pyrrol−Si(HIPE)	39.18(39.6)	1.92(1.94)	$SiO_{1.907}(C_7H_{10}N)_{0.093}(C_{17}H_{38}NBr)_{0.09}\cdot 0.11H_2O$
methyl−Si(HIPE)	21(20.73)	2(2)	$SiO_{1.885}(CH_3)_{0.115}(C_{17}H_{38}NBr)_{0.042}\cdot 0.09H_2O$
dinitro−Si(HIPE)	33.6(33.7)	2.42(2.3)	$SiO_{1.94}(C_9H_{10}O_4N_3)_{0.06}(C_{17}H_{38}NBr)_{0.05}\cdot 0.12H_2O$
benzyl−Si(HIPE)	27(27.39)	2.09(2.08)	$SiO_{1.9127}(C_7H_7)_{0.088}(C_{17}H_{38}NBr)_{0.045}\cdot 0.10H_2O$
mercapto−Si(HIPE)	28.27(28.20)	1.2(1.24)	$SiO_{1.894}(C_3H_7S)_{0.106}(C_{17}H_{38}NBr)_{0.047}\cdot 0.06H_2O$

[a] The number in parentheses corresponds to the weight loss calculated while the number free of parentheses corresponds to the values extracted from the TGA curves. [b] The presented weight loss values are extracted from TGA experiments (Figure 1, Supporting Information).

of each signal appearing in the simulations. Similar line width values were used in each spectrum to minimize quantification errors. In this table, the chemical shift of the different T and Q units for all systems is specified, underlining the above-mentioned effect of the organic substituent on the T^n chemical shift, as a difference of the Q^n units.

The distribution of T^n ($T^2 + T^3$) and Q^n ($Q^2 + Q^3 + Q^4$) units in the final materials obtained by ^{29}Si NMR experiments was calculated and compared with that expected from the molar ratio of the initial precursors (Table 5).

They are in perfect agreement, revealing that this synthesis method provides good control of the composition of the final material. The evaluation of the global condensation degree (C.D.) of the materials has been performed by applying the formula

$$\text{C.D.} = (2\cdot\%T^2 + 3\cdot\%T^3 + 2\cdot\%Q^2 + 3\cdot\%Q^3 + 4\cdot\%Q^4)/(3\cdot\%T + 4\cdot\%Q)$$

The percentage of condensation for the hybrid networks ranges between 87.2% and 89%, in the following order: methyl > benzyl > mercapto > dinitro > pyrrol. These values are acceptable results taking into account that these materials present a real functionality of about 2[2] and they have been prepared in highly acidic conditions. Similar formulas can be used to evaluate the C.D. of Q units (C.D.^{Q}) and T units (C.D.^{T}). From these values, it can be inferred that condensation of the T units (92.2−94.4) has been more effective than that of Q units (86.3−88.1). This behavior can be explained by the well-known higher reactivity of organosilane precursors than TEOS,[32] even in the systems with important steric hindrances.

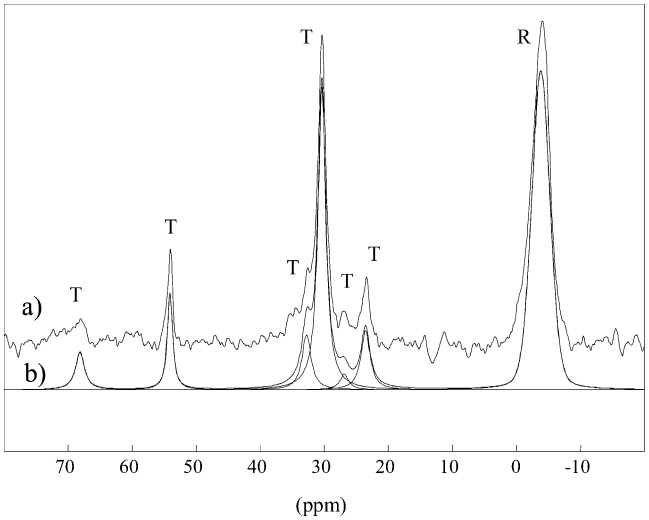

Figure 7. Experimental and simulated ^{13}C CP MAS NMR spectra of methyl−Si(HIPE). TTAB peaks are noted T and R−silane peaks are noted R. (a) experimental spectrum; (b) simulated.

At the molecular level, it seems important to prove that the organic functions remain intact through the applied thermal treatment, 180 °C for 6 h in air. In this issue ^{13}C CP MAS NMR experiments were undertaken; an example is shown for the methyl−Si(HIPE) sample (Figure 7). The R−silane group peak (noted R) and the TTAB peaks (noted T) have been attributed. All the expected peaks are present, except the end chain methyl on TTAB because of its higher mobility. This fact proves the integrity of the introduced components, as also discussed later within the FTIR section. Even if the CP-MAS is not quantitative, deconvolution of the spectra can give an estimation of the TTAB content. For the methyl−Si(HIPE) sample, the comparison of the areas of the TTAB peak at 30.4 ppm (27.2% which accounts for eight carbons) and of the R−Si peak at −3.8 ppm (49.3% which accounts for one carbon) give a TTAB content of 6.5 ± 2%. Similar or inferior results were obtained for the other materials (not shown). Different contact times were tested, showing that the contact time of 1 ms used permitted the results to be nearly quantitative. To address better quantitative results, we have performed TGA experiments (TGA curves presented within the Supporting Information, Figure 1). The ^{29}Si NMR results, which allow quantifying the organo−silane condensation yield, will provide the $SiO_{(2-x)}R_x$ ratio. In a second step considering the TGA performed in air (see Experimental Section for details), the first weight loss from 25 to 150 °C will provide the amount of H_2O, while the second weight loss from 150 to 650 °C will quantify the total organic counterpart present in the compounds. The difference of the total organic weight loss assessed by the TGA experiments with the $SiO_{(2-x)}R_x$ ratio provided by the ^{29}Si NMR results will allow quantifying the amount of TTAB still present within the materials. Final stoichiometries will

(32) Van Blaaderen, A.; Kentgens, A. P. M. *J. Non-Cryst. Solids* **1992**, *149*, 161.

be expressed within the following format: $SiO_{(2-x)}R_x(TTAB)_y \cdot nH_2O$ and are presented in Table 6.

Beyond solid-state NMR and TGA experiments, we have performed some Fourier transformed infrared spectroscopy (FTIR) analyses to prove the organo−silane integrity upon the synthetic and thermal treatment used; all the spectra are represented within Figure 8.

First, all the spectra have in common a strong absorption centered at 1076 cm^{-1} that correspond to the ν(Si−O) stretching modes. The second vibration mode present in all the spectra is the one involving the stretching mode of the Si−C link occurring within the 900−700 cm^{-1} region. The ν(Si−C) stretching mode is considerably influenced by the nature of the substitute groupings; thus, the Si−C stretching mode for the pyrrol−Si(HIPE), methyl−Si(HIPE), dinitro−Si(HIPE), benzyl−Si(HIPE), and mercapto−Si(HIPE) is appearing respectively at 786, 803, 789, 793, and 794 cm^{-1}. Also, the silanol (Si−OH) vibrations mode is present at around 3250 cm^{-1}, generating a superimposed shoulder among the resonance structures (hydrogen bonds) of the adsorbed water OH stretching modes (broader band ranging from 3200 to 3600 cm^{-1}). Also, each spectra possess strong IR absorption at 2927 and 2858 cm^{-1} that correspond respectively to the symmetric $\nu_s(CH_2)$ and asymmetric $\nu_{as}(CH_2)$ stretching mode of the TTAB alkyl tails. This feature is proving that the TTAB surfactant is maintained within the organo−Si(HIPE) core and thus perturbing the surface areas access by nitrogen sorption measurements. More independently, each of the silane organic moieties should promote specific absorption modes acting as a molecules signature. Considering the molecular configuration of the pyrrol derivatives (Scheme 1), the pyrrol−Si(HIPE) compounds will depict the same four aromatic ν(C═C) stretching modes between 1450 and 1650 cm^{-1} as the benzyl−SiHIPE compound. Therefore, the intrinsic signature of the pyrrol moieties will emerge from the C−N bond. Taking into account Figure 8a (embedded), we can observe the ν(C−N) stretching of the tertiary amine at 1360 cm^{-1}. Also, we can observe a relatively strong absorption at 1658 cm^{-1}, which is a consequence of the $\delta(NH^+)$ associated with a rocking NH^+ vibration occurring at 795 cm^{-1}. These vibration modes demonstrate that the tertiary amino groups born by the pyrrol moieties are protonated, as discussed within the section dealing with the characterization at the mesoscale level. The methyl−Si(HIPE) FTIR spectrum is associated with specific CH_3 stretching modes, symmetric (ν_s) and asymmetric (ν_{as}), arising respectively at 2856 and 2932 cm^{-1} (Figure 8b, embedded). The FTIR spectrum of the dinitro−Si(HIPE) compound possesses also the four aromatic ν(C═C) stretching modes between 1450 and 1650 cm^{-1}. In addition, strong absorption bands specific to symmetric ν_s (NO_2) and asymmetric $\nu_{as}(NO_2)$ stretching modes are appearing at 1338 and 1585 cm^{-1}, respectively (Figure 8c, embedded). Also, a strong absorption at 1622 cm^{-1} which addresses the $\delta(NH_2^+)$ deformation band (Figure 8c, embedded) combined with a rocking NH_2^+ vibration occurring at 807 cm^{-1} demonstrate that the secondary amine born by the dinitrophenylamino moieties is indeed protonated. Concerning the benzyl−Si-

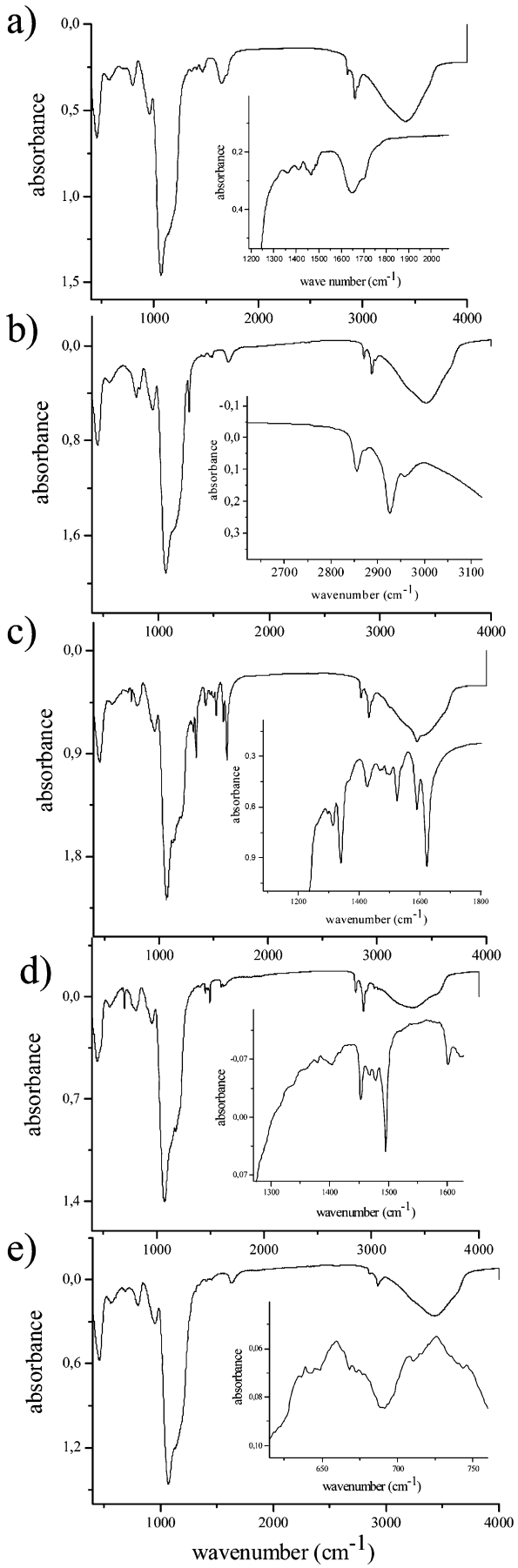

Figure 8. Organo−SiHIPE FTIR spectra: (a) pyrrol−Si(HIPE), (b) methyl−Si(HIPE), (c) dinitro−Si(HIPE), (d) benzyl−Si(HIPE), and (e) mercapto−Si(HIPE).

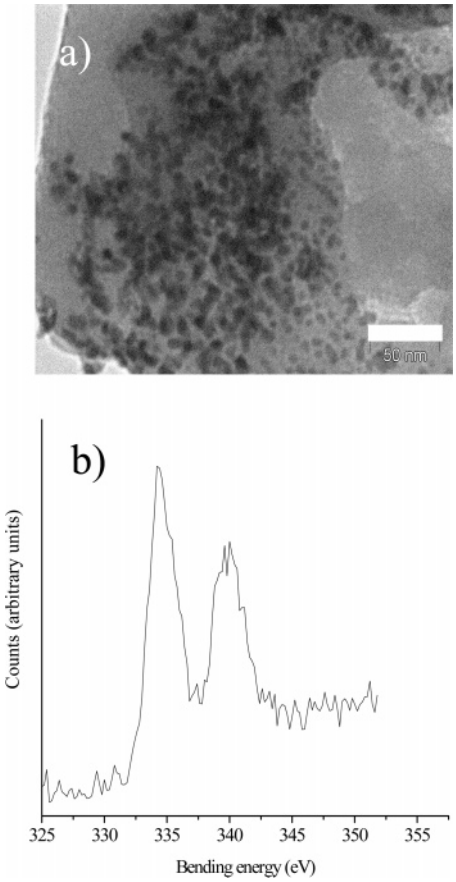

Figure 9. Pd heterogeneous nucleation within the mercapto−Si(HIPE) compound. (a) TEM visualization, the scale bar represents 50 nm. (b) XPS spectrum of the mercapto−Si(HIPE) compound bearing Pd nanoparticles.

(HIPE) compound, FTIR signature will emerge from the aromatic ν(C═C−C) and associated νC═(C−H) stretching modes. The typical aromatic (C═C−C) stretching modes is present with a group of four bands between 1450 and 1650 cm^{-1} (Figure 7d, embedded) and associated with the νC═(C−H) sharp absorption at 3050 cm^{-1}. Also bands appear in the region 1000−650 cm^{-1} due to the δC═(C−H) out-of-plane deformation vibrations of the hydrogen atoms localized on the ring. Finally, the typical signature of the mercapto−Si(HIPE) compound will emerge from the C−S bond, absorption that is known to be weak. Effectively, the ν(C−S) stretching mode can be observed at 690 cm^{-1} and is associated with a weak absorption (Figure 8e, embedded). Also, a weak S−H stretching mode is present at 2560 cm^{-1}. Overall, the FTIR results are proving that the organic moieties of these new open-cell materials remain intact through the employed synthetic route.

Molecular Function Accessibility. Beyond the synthesis and characterizations at several length scales of this new set of trimodal porous monolith-type architectures, it seems obvious to prove the molecular function accessibility. To witness this accessibility, we made use of Pd nanoparticles heterogeneous nucleation, with functional porous monolith-type materials that is potentially bearing the abilities to both promote metallic heterogeneous nucleation and offer the capability to stabilize the metal particle into its zerovalent state nature. For this purpose we chose to test the mercapto−Si(HIPE) compound. As observed, in Figure 9a Pd nanoparticles have been generated, with average size diameters around 4−6 nm.

At this stage, bearing in mind that the inorganic surface alone can act as a defect to minimize the nucleation enthalpy, thus being able to promote nucleation, the TEM contemplative issue is not enough by itself to prove the molecular function accessibility. Concerning the Pd heterogeneous nucleation, and considering previous work performed within nonfunctionalized organic PolyHIPE,[33] the as-synthesized particles were in fact a core−shell composed of a thin layer of palladium oxide with a zerovalent Pd core. As expressed within Figure 9b, this is not what we obtained here. The Pd XPS spectrum possesses two peaks centered at 335 and 340.3 eV that correspond respectively to the $3d_{5/2}$ and $3d_{7/2}$ of metallic zerovalent Pd nanoparticles.[34] Both TEM and XPS are thus witnessing that the mercapto molecular function is therefore accessible to both promotion of the Pd heterogeneous nucleation and offering of a good stabilizing effect, which enables keeping all the Pd metallic nanoparticles in the zerovalent state.

Conclusion

Organo−silica monoliths with hierarchical bimodal porous structures are obtained for the first time via both HIPE phases process, lyotropic mesophases and sol−gel chemistry, fitting thus the integrative chemistry synthetic route.[17] The resulting hybrid compounds, which we aimed to label organo−Si-(HIPE) materials, exhibit micrometric void spaces combined with a mesoscopic porosity that varies from wormlike to hexagonal depending on the organic functionality. Shaped hybrid monoliths with good mechanical integrity are presenting average condensation degree ranging between 86 and 90% while maintaining the organic moieties intact through the entire process in use. Beyond, through the use of Pd heterogeneous nucleation the molecular function accessibility has been demonstrated. These open-cell hybrid organo−Si-(HIPE) monoliths, bearing methyl, benzyl, mercapto, dinitrophenylamino, or pyrrol moieties, are of potential interest for multiple applications in heterogeneous catalysis, separation techniques, absorbers, sensors, and so forth. Next work will be dedicated to tuning the Pd derivative materials toward heterogeneous catalysis reactions; this work is underway and will be published in due time.

Acknowledgment. This work is part of the FAME-MIOH 6-PCRDT program.

Supporting Information Available: Thermogravimetric analyses (TGA). This material is available free of charge via the Internet at http://pubs.acs.org.

CM701984T

(33) Desforges, A.; Deleuze, H.; Mondain-Monval, O.; Backov, R. *Ind. Eng. Chem. Res.* **2005**, *44*, 8521.
(34) Brun, M.; Berthet, A.; Bertolini, *J. Electron Microsc. Relat. Phenom.* **1999**, *104*, 55.